IEEE 802.11ac: Performance of MU-MIMO Interference Cancellation Detectors with Imperfect Channel State Information at Tx and Rx Sides

Roger Pierre Fabris Hoefel

Electrical Engineering Department
Federal University of Rio Grande do Sul (UFRGS)
Porto Alegre, RS, Brazil
roger.hoefel@ufrgs.br

Oscar Bejarano

Electrical and Computer Engineering Department
Rice University
Houston, TX, USA
obejarano@rice.edu

Abstract— **In this paper we analyze the performance of IEEE 802.11ac downlink multi-user multiple input multiple output (MU-MIMO) transceiver architectures that implement regularized channel inversion minimum mean squared error (RI-MMSE) precoder at transmitter (TX) and interference cancellation (IC) MMSE MIMO detector at receiver (RX). IEEE 802.11ac simulation results, assuming imperfect channel state information (CSI) at both TX and RX sides over spatial-correlated and frequency selective TGac MIMO channels, have shown that the use of spatial degrees of freedom to cancel inter-stream interference can mitigate the negative effects of imperfect synchronization and channel estimation, and channel sounding feedback delays in IEEE 802.11ac systems. Simulation results have also shown that single-user MIMO 802.11ac systems with transmit beamforming achieve higher performance compared to MU-MIMO systems with IC-MMSE MIMO detectors when sounding feedback delays and CSI imperfections are taken into account.**

I. Introduction

The IEEE 802.11ac standard amendment [1-2] has specified the optional implementation of downlink (DL) multi-user multiple input multiple output (MU-MIMO) technology. This technique aims at improving the system throughput when the system is loaded with small form factor stations (STAs) and, consequently, a smaller number of receive antennas with relation to (w.r.t.) the number of transmit antennas deployed at the access points (APs). This typical scenario does not allow to use all degrees of freedom of the MIMO channel if only single-user (SU) MIMO techniques are implemented

The 802.11ax Task Group (TG), created in March 2014 [3], has focused on increasing per area throughput efficiency in dense networks deployed in outdoor and indoor environments with major concerns about power consumption, instead of focusing in per-link throughput in indoor networks as in the earlier 802.11 specifications. Currently, TGax is considering multiple physical layer (PHY) techniques for the inclusion in the amendment, such as downlink and uplink (UL) MU-MIMO, orthogonal frequency division multiple access (OFDMA), massive MIMO, MIMO precoding, long cyclic prefix (CP), fractional frequency reuse, full-duplex. In this paper we focus on interference cancellations techniques and investigate their impact on DL MU-MIMO performance. We argue that these techniques are highly relevant to the next generation 802.11ac/ax chipsets.

The design of interference cancellation minimum mean squared error (IC-MMSE) MIMO detectors for 802.11ac-based DL MU-MIMO was proposed by *Qualcomm* in [4], which led to the introduction of the resolvable very-high throughput long-training field (VHT-LTF) in the 802.11ac PHY preamble, as described in Section II. However, the results shown in [4] are only based on *Shannon capacity* gains due to signal-to-interference-plus-noise ratio (SINR) improvements of IC-MMSE MIMO detector implementation. In contrast to this paper, no *realistic scenario*s with complete 802.11ac PHY simulation are shown in [4].

The remaining of this paper is organized as follows: Section II describes in great detail the design of IEEE 802.11ac DL MU-MIMO transceivers that implement regularized channel inversion minimum mean squared error (RI-MMSE) precoder and IC-MMSE MIMO detector at transmitter (TX) and receiver (RX) sides, respectively. Section III presents a consistent set of 802.11ac simulation results that allow comparing the performance of the following transceiver architectures: *(i)* MU-MIMO transceiver with RI-MMSE precoder and CI-MMSE MIMO detector; *(ii)* MU-MIMO transceiver with RI-MMSE precoder and MMSE MIMO detector; *(iii)* single user (SU) MIMO with adaptive transmit beamforming (TxBF) and MMSE MIMO detector; *(iv)* SU-MIMO with fixed spatial expansion (SE) precoder and MMSE MIMO detector. This sections contains our *main contributions,* i.e., the assessment of aforementioned 802.11ac MU and SU MIMO transceivers performance considering realistic schemes for synchronization, channel state information (CSI) and sounding over spatial-correlated and frequency selective TGac channel models. Section IV presents our conclusions.

Finally, we have acknowledge that the subject of interference cancellation in MU-MIMO systems has been a topic of active research [5-7]. However, there is still room for R&D papers (e.g., only hard-decision Viterbi decoding without Doppler effects is assumed in [5]) that present an unified performance analyzes of IC-MMSE MIMO detectors for MU-MIMO assuming realistic 802.11ac systems, as we develop in this paper.

II. Downlink MU-MIMO: Transceiver Design

Signal processing operations are performed per subcarrier in the MIMO-OFDM PHY. In order to simplify the notation, we omit the index that specifies the subcarrier being processed when this can be perfectly inferred from the context.

A. Received Signal Model

In the frequency domain, the received symbols over the DL MU-MIMO OFDM channel can be modeled as

$$\boldsymbol{y} = \begin{bmatrix} \boldsymbol{y_1} \\ \boldsymbol{y_2} \\ \vdots \\ \boldsymbol{y_K} \end{bmatrix} = \boldsymbol{H_{DL}x} + \boldsymbol{z} = \begin{bmatrix} \boldsymbol{H_1} \\ \boldsymbol{H_2} \\ \vdots \\ \boldsymbol{H_K} \end{bmatrix} \cdot \left[x_1 x_2 \cdots x_{n_{ss,total}}\right]^T + \begin{bmatrix} \boldsymbol{z_1} \\ \boldsymbol{z_2} \\ \vdots \\ \boldsymbol{z_K} \end{bmatrix}, \qquad (1)$$

where K is the number of users. The DL MU-MIMO channel is modeled by the matrix $\mathbf{H_{DL}}$ with size $n_{r,total} = \sum_{u=1}^{K} n_{r,u}$ by n_t,

978-1-4673-8451-3/15/$31.00 ©2015 IEEE

where $n_{r,u}$ is the number of receive antennas of the uth station (STA) and n_t is the number of transmit antennas. The DL MIMO channel matrix of the uth user is denoted by $\mathbf{H_u}$ and it has size of $n_{r,\mathrm{u}}$ by n_t [8, pp. 401].

The received signal observed by the uth user is given by

$$\boldsymbol{y_u} = \boldsymbol{H_u x} + \boldsymbol{z_u}, \quad \mathrm{u} = 1, \cdots \mathrm{K}. \tag{2}$$

The symbols at the output of the transmit antenna elements are given by $\boldsymbol{x} = \boldsymbol{P} \cdot \boldsymbol{s}$, where $\mathbf{P}$ is the pre-coding matrix with size n_t by $n_{ss,total} = \sum_{u=1}^{K} n_{ss,u}$, where $n_{ss,u}$ is the number of spatial streams (SS) transmitted to the uth STA. Notice that $n_{ss,total}$ denotes the total number of SS transmitted to all K STAs. The transmitted symbols for all K users are denoted using the column vector $\mathbf{s}= \left[\mathbf{s_{u,1}^T}, \mathbf{s_{u,2}^T}, \cdots \mathbf{s_{u,K}^T}\right]^{\mathbf{T}}$, where the symbols transmitted to the uth STA are modeled by the column vector $\boldsymbol{s_u} = \left[s_{u,1}, s_{u,2}, \cdots, \mathrm{s}_{u,n_{ss,u}}\right]^{\boldsymbol{T}}$. The downlink transmitted symbol to the uth user at jth SS is denoted by $s_{u,j}$.

The zero mean circular symmetric complex Gaussian (ZMCSCG) is modeled by the column vector **z.** This vector is formed by K random vectors, where each column vector $\boldsymbol{z}_u = \left[\mathrm{z}_{\mathrm{u},1}, \mathrm{z}_{\mathrm{u},2}, \cdots \mathrm{z}_{\mathrm{u},\mathrm{n_{ru}}}\right]^{\boldsymbol{T}}, u = 1, \cdots K,$ is composed by $z_{u,j}\,(j = 1, .. n_{r,u})$ independent and identical distributed (i.i.d.) ZMCSCG random variables (r.v.) with variance N_0.

B. Sounding and Channel Estimation

Eq. (1) models the received signal when pre-coding is implemented at TX side. In this section, we describe the procedures implemented in 802.11ac to estimate the MIMO channel matrix necessary to determine the precoding matrix **P**.

The IEEE 802.11ac standard amendment specifies that the AP must sound explicitly the channel in order to obtain the CSI used to calculate the precoding matrix **P**. Fig. 1 shows that the AP (beamformer) first transmits the null-data packet announcement (NDPA) that identifies the STAs (or beamformees) involved in the current sounding procedure [9]. After the short interframe space (SIFS), the beamformer transmits the null-data packet (NDP) that contains the VHT-LTF used by the beamformees to estimate the channel. Next, the first beamformee specified in the NDPA transmits representation of its estimated CSI using a compressed beamforming frame. Notice that the compressed beamforming frame contains the parameters used to compress the feedback via Givens rotations [2, pp. 388] and it also includes estimates of both average signal-to-noise ratio (SNR) and SNR per subcarrier [2, pp. 438], [6]. Continuing this procedure, the beamformer transmits the beamforming reporting poll that simultaneously acknowledge (ACK) the received compressed beamforming frame and poll the next STA. This procedure continuous until all the STAs involved in the sounding procedure are polled in to feedback their estimated CSI to the AP.

The PHY preamble of NDP and data frames used to transmit medium access control packet data units (MPDU) contains the VHT-LTF, which carries known pilots $\mathrm{VHTLF}^{(k)}$ transmitted at kth subcarrier. Notice that the VHT-LTF is the same for all users involved in the MU-MIMO transmission and that during the sounding procedure the precoding is not implemented.

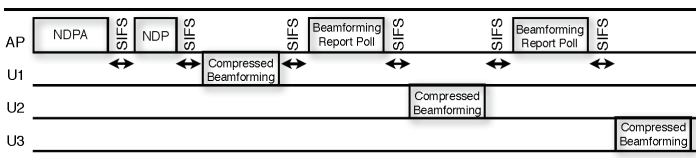

Figure 1. Temporal sequences of 802.11ac frames for MU-MIMO sounding.

The number of transmitted VHT-LTF OFDM symbols in the NDP is given by [2, pp. 431]

$$N_{LTF} = \begin{cases} n_{ss,total} & if\ n_{ss,total} = 1,2,4,6,8 \\ n_{ss,total} + 1 & if\ \ n_{ss,total} = 3,5,7 \end{cases}. \tag{3}$$

Eq. (3) shows that the number of VHT-LTF in the NDP frame depicted in Fig. 1 depends on the channel dimensionality to be sounded [2, pp. 379]. For instance, considering a typical system configuration with four transmit antennas at AP and four STAs with two receive antennas each, it is necessary to transmit eight LTF if two SSs are transmitted for each STA, whilst only four LTF are necessary if only one SS is transmitted per STA.

It is shown in [2, pp. 98] that the normalized least square (LS) estimation matrix for the kth subcarrier during the sounding procedure is given by

$$\begin{bmatrix} \hat{h}_{11}^{(k)} & \hat{h}_{12}^{(k)} & \cdots & \hat{h}_{1n_t}^{(k)} \\ \hat{h}_{21}^{(k)} & \hat{h}_{22}^{(k)} & & \hat{h}_{2n_t}^{(k)} \\ \vdots & & \ddots & \vdots \\ \hat{h}_{n_{ss,u}1}^{(k)} & \hat{h}_{n_{ss,u}2}^{(k)} & \cdots & \hat{h}_{n_{ss,u}n_t}^{(k)} \end{bmatrix} = [\boldsymbol{y}_{t_1}^{(k)}, \boldsymbol{y}_{t_2}^{(k)}, \cdots \boldsymbol{y}_{N_{LTF}}^{(k)}][\widetilde{\boldsymbol{V}}_{\boldsymbol{VHTLF}}(\mathbf{1}: \boldsymbol{n_t}, \mathbf{1}: \boldsymbol{N_{LTF}})]^T \frac{1}{\mathrm{VHTLF^{(k)} \cdot N_{LTF}}}, \tag{4}$$

where $\widetilde{\boldsymbol{V}}_{\boldsymbol{VHTLF}}(1{:}n_t, 1{:}N_{LTF})$ is an subset with the first n_t rows and N_{LTF} columns of the orthogonal cover matrix (OCM) **V** [2, pp. 88, pp. 198]. The frequency response between the ith receive antenna and the jth transmit antenna for the kth subcarrier is denoted by $\hat{h}_{ij}^{(k)}$, where the superscript hat is used to indicate that the effects of CSI, imperfect time and frequency synchronization are included in the observed channel response in the frequency domain. The $\mathrm{VHTLF}^{(k)}$ denotes the known pilot transmitted at kth subcarrier. The OCM $\mathbf{V}_{\mathrm{VHTLF}}$ is unitary, i.e., $\boldsymbol{V}_{VHTLF} \cdot \boldsymbol{V}_{VHTLF}^{T} = \boldsymbol{I}_{N_{LTF}}$, where the $(.)^{\mathrm{T}}$ indicates the transpose operation. Notice that during the sounding procedure the receiver of uth STA only processes the signal received in $n_{ss,u}$ of its $n_{r,u}$ antennas (where $n_{ss,u}$ is less or equal to $n_{r,u}$) since the precoding matrix **P** used in (1) has size n_t by $n_{ss,total} = \sum_{u=1}^{K} n_{ss,u}$. Hence, the column vector $\boldsymbol{y}_{t_m}^{(k)}$ has dimension $n_{ss,u}$ and it contains the received signal for the mth VHT-LTF ($\mathrm{m=1,...,N_{LTF}}$) in the kth subcarrier.

The procedure described above applies to the VHT-LTF transmitted in the NDP during the sounding procedure. However, it is also applied to the VHT-LTF transmitted in preamble of MPDU with the following changes: *(i)* the estimated channel matrix includes the effects of precoding on the effective channel matrix observed for each user; (*ii*) the column vector $\boldsymbol{y}_{t_m}^{(k)}$ has now dimension equal to the number of receive antennas of the uth STA (i.e., $n_{r,u}$) since the MIMO detector must use all the available CSI at RX side to improve its performance.

C. MU-MIMO Precoding

Assuming that all users have the same average signal-to-noise ratio (SNR), then the RI-MMSE precoding matrix is given by (5), where $\mathbf{I}_{n_{ss,total}}$ denotes a diagonal matrix with dimension $n_{ss,total}$. The normalization factor of the transmitted power is given by (6). The RI-MMSE decreases the noise enhancement when the channel inversion zero forcing (ZF) precoder is used over DL MU-MIMO channels whose eigenvalues have a large spread [10].

$$\boldsymbol{P_{MMSE}} = \beta_{\mathrm{MMSE}} \cdot \widehat{\boldsymbol{H}}_{\boldsymbol{DL}}^{\boldsymbol{H}} \cdot \left[\widehat{\boldsymbol{H}}_{\boldsymbol{DL}} \cdot \widehat{\boldsymbol{H}}_{\boldsymbol{DL}}^{\boldsymbol{H}} + \frac{1}{\mathrm{SNR}} \mathbf{I}_{n_{ss,total}}\right]^{-1}. \tag{5}$$

$$\beta_{MMSE} = \sqrt{\frac{\mathrm{n_t}}{\mathrm{trace}(\boldsymbol{P_{MMSE}} \cdot \boldsymbol{P_{MMSE}^H})}}. \tag{6}$$

Notice that in a typical MU-MIMO configuration, the TX transmits a number of SS equal to the number of transmit antennas and the RX has more antennas than the number of SSs in order to have degrees of freedom to cancel the leak of MU

interference due to imperfect precoding. In this case, the channel matrix feed back per each user during the sounding procedure has dimension $n_{ss,u}$ by n_t and, therefore, the matrix $\widehat{\boldsymbol{H}}_{\boldsymbol{DL}}$ used in (5) has size $n_{ss,total}$ by n_t . The matrix **P** has dimension n_t by $n_{ss,total}$.

D. TGac Channel Model

The simulation results presented in this paper assume the spatial correlated and frequency selective TGac D channel model [11]. This typical office channel model has three clusters, maximum excess delay of *390 ns* and root mean square (rms) delay spread of *50 ns* [2, pp. 38]. A description on the implementation of TGac channel models in the 802.11c simulator can be found in [12].

In this paper, we investigate the effects of the channel sounding delay on the performance of DL MU-MIMO transceivers. In order to accomplish it, the Doppler power spectrum (DPS) in TGn MIMO channel model is modeled by [2, pp 45]

$$S_d(f) = \frac{\sqrt{A}/(\pi f_d)}{1+A\left(\frac{f}{f_d}\right)}, \quad |f| \le f_{max}, \tag{7}$$

where $\boldsymbol{f_d} = \frac{v}{c}\boldsymbol{f_c}$ denotes the Doppler spread; f_c denotes the carrier frequency in Hz; c the speed of light and v_0 is the environmental speed (i.e., v_0 is fixed in *1.2 km/h*, given $\boldsymbol{f_d} \cong \boldsymbol{6\ Hz\ at\ 5\ GHz\ band}$). The *constant A* equal to *9* means that the spectrum is *10 dB* below the peak at Doppler spread frequency.

The TGac has modified the environmental speed to *0.089 km/h* due to measurements that have indicated that the 802.11n model is more suitable to mobile devices. This results in a channel coherence time of *800 ms* at f_c*=5.25 GHz* [2, pp, 46].

E. MU-MIMO Detector

The received signal vector at the output of the MIMO detector for the *u*th STA is given by (8), where the received signal for the *u*th STA is given by (2) and the matrix $\mathbf{W_u}$ stands for the linear filter for the u*th* STA. Notice the matrix $\mathbf{W_u}$ has size $n_{r,u}$ by $n_{ss,u}$.

$$\tilde{\boldsymbol{y}}_{\boldsymbol{u}} = \boldsymbol{W}_{\boldsymbol{u}}^{\boldsymbol{H}}\boldsymbol{y}_{\boldsymbol{u}} = \boldsymbol{W}_{\boldsymbol{u}}^{\boldsymbol{H}} \cdot (\boldsymbol{H}_{\boldsymbol{u}}\boldsymbol{P}\boldsymbol{s} + \boldsymbol{z}_{\boldsymbol{u}}). \tag{8}$$

Eq. (9) can be expanded in order to differentiate between the signal transmitted to the *u*th and to the remaining users, i.e.,

$$\tilde{\boldsymbol{y}}_{\boldsymbol{u}} = \boldsymbol{W}_{\boldsymbol{u}}^{\boldsymbol{H}} \cdot (\boldsymbol{H}_{\boldsymbol{u}}\boldsymbol{P}_{\boldsymbol{1}}\boldsymbol{s}_{\boldsymbol{1}} + \cdots + \boldsymbol{H}_{\boldsymbol{u}}\boldsymbol{P}_{\boldsymbol{u}}\boldsymbol{s}_{\boldsymbol{u}} + \cdots + \boldsymbol{H}_{\boldsymbol{u}}\boldsymbol{P}_{\boldsymbol{K}}\boldsymbol{s}_{\boldsymbol{K}} + \boldsymbol{z}_{\boldsymbol{u}}), \tag{9}$$

where $\mathbf{P_u}$, with dimension n_t by $n_{ss,u}$, denotes the columns of the matrix **P** used to precoding the symbols transmitted to the *u*th STA. Denoting the effective channel matrix observed by *u*th user as $\widetilde{\boldsymbol{H}}_{\boldsymbol{u}} = \boldsymbol{H}_{\boldsymbol{u}}\boldsymbol{P}$, then (8) and (9) can be conveniently rewritten as (11) and (12), respectively**.**

$$\widetilde{\boldsymbol{H}}_{\boldsymbol{u}} = [\boldsymbol{H}_{\boldsymbol{u}}\boldsymbol{P}_{\boldsymbol{1}}, \cdots \boldsymbol{H}_{\boldsymbol{u}}\boldsymbol{P}_{\boldsymbol{u}}, \cdots, \boldsymbol{H}_{\boldsymbol{u}}\boldsymbol{P}_{\boldsymbol{K}}] = [\widetilde{\boldsymbol{H}}_{\boldsymbol{u},\boldsymbol{1}}, \cdots \widetilde{\boldsymbol{H}}_{\boldsymbol{u},\boldsymbol{u}}, \cdots, \widetilde{\boldsymbol{H}}_{\boldsymbol{u},\boldsymbol{k}}]. \tag{10}$$

$$\tilde{\boldsymbol{y}}_{\boldsymbol{u}} = \boldsymbol{W}_{\boldsymbol{u}}^{\boldsymbol{H}} \cdot (\widetilde{\boldsymbol{H}}_{\boldsymbol{u}}\boldsymbol{s} + \boldsymbol{z}_{\boldsymbol{u}}). \tag{11}$$

$$\tilde{\boldsymbol{y}}_{\boldsymbol{u}} = \boldsymbol{W}_{\boldsymbol{u}}^{\boldsymbol{H}} \cdot (\widetilde{\boldsymbol{H}}_{\boldsymbol{u},\boldsymbol{1}}\boldsymbol{s}_{\boldsymbol{1}} + \cdots + \widetilde{\boldsymbol{H}}_{\boldsymbol{u},\boldsymbol{u}}\boldsymbol{s}_{\boldsymbol{u}} + \cdots + \widetilde{\boldsymbol{H}}_{\boldsymbol{u},\boldsymbol{K}}\boldsymbol{s}_{\boldsymbol{K}} + \boldsymbol{z}_{\boldsymbol{u}}). \tag{12}$$

If it is assumed that the MU interference is perfectly cancelled by the precoder, then (12) is simplified to

$$\tilde{\boldsymbol{y}}_{\boldsymbol{u}} = \boldsymbol{W}_{\boldsymbol{u}}^{\boldsymbol{H}} \cdot (\widetilde{\boldsymbol{H}}_{\boldsymbol{u},\boldsymbol{u}}\boldsymbol{s}_{\boldsymbol{u}} + \boldsymbol{z}_{\boldsymbol{u}}). \tag{13}$$

Using (13), the MMSE MIMO detector to the *u*th user is given by

$$\boldsymbol{W}_{\boldsymbol{MMSE},\boldsymbol{u}} = \widetilde{\boldsymbol{H}}_{\boldsymbol{u},\boldsymbol{u}} \cdot \left(\widetilde{\boldsymbol{H}}_{\boldsymbol{u},\boldsymbol{u}}^{\boldsymbol{H}}\widetilde{\boldsymbol{H}}_{\boldsymbol{u},\boldsymbol{u}} + \frac{\boldsymbol{I}_{\boldsymbol{n_{ss,u}}}}{\boldsymbol{SNR}_{\boldsymbol{u}}}\right)^{-\boldsymbol{1}}. \tag{14}$$

However, if the imperfect cancellation of MU interference is taken into account, then using (12) the MMSE MIMO detector is given by [5]

$$\boldsymbol{W}_{\boldsymbol{MMSE},\boldsymbol{u}} = \widetilde{\boldsymbol{H}}_{\boldsymbol{u},\boldsymbol{u}} \cdot \left[(\widetilde{\boldsymbol{H}}_{\boldsymbol{u}})^{\boldsymbol{H}}\widetilde{\boldsymbol{H}}_{\boldsymbol{u}} + \frac{\boldsymbol{I}_{\boldsymbol{nSS,total}}}{\boldsymbol{SNR}_{\boldsymbol{u}}}\right]^{-\boldsymbol{1}}. \tag{15}$$

According with (14), each STA involved in MU-MIMO transmission needs only to estimate the matrix $\widetilde{\boldsymbol{H}}_{\boldsymbol{u},\boldsymbol{u}}$ if the MU-MIMO interference is neglected. Therefore, the number of the VHT-LTF to estimate the channel in the sounding procedure should be equal to the number of SSs transmitted to the *u*th user since the matrix $\widetilde{\boldsymbol{H}}_{\boldsymbol{u},\boldsymbol{u}}$ has size $n_{r,u}$ by $n_{ss,u}$. However, if the MMSE MIMO detector takes the MU-MIMO interference into account, then (15) shows that the VHT-LTF must have a number of SSs specified by (3), i.e., the SSs transmitted to all users must be considered in order to estimate the matrix $\widetilde{\boldsymbol{H}}_{\boldsymbol{u}} = \boldsymbol{H}_{\boldsymbol{u}}\boldsymbol{P}$ with size $n_{r,u}$ by $n_{ss,total}$ [2, pp. 431], [5].

III. Performance Analyzes

Tab. I shows the main characteristics of the IEEE 802.11ac simulator, which is described and validated in [12]. In this paper, we have assumed f_c=5.25 GHz with v_0 equal to 1.2 km/h, which generate a MIMO channel with coherence time of 50 ms when correlation of 50% is assumed. Notice that these parameters create a DPS that allows to investigate the performance of MU-MIMO transceivers over pedestrian speeds according with TGn. It is implemented the soft-output demmaper for binary interleaved code modulation (BICM) proposed in [13].

Table I– Basic parameters of IEEE 802.11ac simulator [12].

Parameter	Value	Parameter	Value
Carrier Frequency	5.25 GHz	MCS	0-9
Bandwidth	20 MHz, 40 MHz, 80 MHz	Number of Spatial Streams	1 to 8
GI Length	800 ns	Synchronization	Auto-Correlation
Modulation	BPSK, QPSK, 16-QAM, 64QAM, 256-QAM	MIMO Channel Estimation	Least Square
Binary Convolutional Code (BCC)	Code rate: r=1/2, r=2/3, r=3/4, r=5/6	Channel Decoder	Hard and Soft-Decision Viterbi Decoding

Tab. II shows the 802.11ac modulation code schemes (MCS) investigated this paper. The selected MCS allows analyzing the performance of modulation and binary convolutional codes (BCC) with the following characteristics: *(i)* antipodal modulation (BPSK) and BCC with industrial standard code rate *r=1/2* (MCS0); *(ii)* constant envelope modulation (QPSK) and BCC with *r=1/2* (MCS1); *(iii)* QPSK and BCC with *r=1/3* (MCS2); *(iv)* medium cardinality non-constant envelope modulation (16-QAM) and BCC with *r=1/2* (MCS3); *(v)* high cardinality non-constant envelope modulation (64-QAM) and BCC with *r=2/3* (MCS5)*; (vi)* 64-QAM and BCC with *r=3/4 (MCS6).*

Table II - MCS investigated in this paper. The PHY data rates assume a guard-interval (GI) of 800 ns and 80 MHz bandwidth (BW).

MCS	Mod	BCC Code Rate	# SSs	Data Rate Mbps
0	BPSK	1/2	1	29.3
			2	58.5
1	QPSK	1/2	1	58.5
			2	117.0
2	QPSK	3/4	1	87.8
			2	175.5
3	16-QAM	1/2	1	117.0
			2	234.0
5	64-QAM	2/3	2	468.0
6	64-QAM	3/4	2	526.5

In this paper, MU-MIMO TGac channels with n_t transmit antennas, and equal number of $n_{r,u}$ receive antennas per each one of the *K* STAS accessing the channel are denoted by *TGac (*n_t *x* $n_{r,u}$ *x K -* $n_{ss,u}$ *SS)*. It is assumed that the same number of SS $n_{ss,u}$ is transmitted for all STAs. The MPDU has a payload of *1500 bytes.*

A. Viterbi Decoding: Soft-Decision Metrics

The output of the MIMO detector for the *i*th SS received by the *u*th STA is given by

$$\tilde{y}_{u,i} = \rho_{u,i}\mathrm{s_{u,i}} + \mathrm{I_{u,i}} + \mathrm{IM_{u,i}} + \tilde{z}_{u,i}, \quad (16)$$

where $u = 1, \cdots, K$ and $i = 1, \cdots, n_{ss,u}$.

The signal and noise components are given by $\rho_{u,i} = \mathbf{w}_{u,i}^H \tilde{\mathbf{h}}_{\mathrm{u,i}}$ and $\tilde{z}_{u,i} = \mathbf{w}_{u,i}^H \boldsymbol{z}_u$, respectively. The spatial signature at the *u*th STA, which includes both the effects of MIMO channel and precoding matrix, due to the symbol transmitted at ith SS is denoted by $\tilde{\mathbf{h}}_{\mathrm{u,i}}$, whilst the weights to detect the *i*th SS transmitted to the *u*th STA are denoted by the column vector $\boldsymbol{w}_{u,i}$ with size $\mathrm{n_{r,u}}$. Notice that $\boldsymbol{W_u} = \boldsymbol{W_{MMSE,u}} = [\boldsymbol{w}_{u,1} \cdots \boldsymbol{w}_{u,n_{ss,u}}]$, i.e., a matrix with dimension $n_{ss,u}$ by $n_{r,u}$.

The interference at the *i*th SS due to other SSs transmitted to the *u*th user is given by (17), while (18) models the multi-user interference observed at *i*th SS of *u*th user.

$$\mathrm{I_{u,i}} = \sum_{\substack{\mathrm{l=1} \\ \mathrm{l\neq i}}}^{\mathrm{n_{ss,u}}} \mathbf{w}_{u,i}^H \tilde{\mathbf{h}}_{\mathrm{u,l}} \mathrm{s_{u,l}}. \quad (17)$$

$$\mathrm{IM_{u,i}} = \sum_{\substack{\mathrm{k=1} \\ \mathrm{k\neq u}}}^{\mathrm{K}} \sum_{\mathrm{j=1}}^{\mathrm{n_{ss,k}}} \mathbf{w}_{u,i}^H \tilde{\mathbf{h}}_{\mathrm{k,j}} \mathrm{s_{k,j}}. \quad (18)$$

The post-detection SINR for the *u*th user at the *i*th SS is given by

$$SINR_{u,i} = \frac{\left|\mathbf{w}_{u,i}^H \mathbf{h}_{\mathrm{u,i}}\right|^2}{\sum_{\substack{\mathrm{l=1} \\ \mathrm{l\neq i}}}^{\mathrm{n_{ss,j}}} \left|\mathbf{w}_{u,i}^H \tilde{\mathbf{h}}_{\mathrm{u,l}}\right|^2 + \sum_{\substack{\mathrm{k=1} \\ \mathrm{k\neq u}}}^{\mathrm{K}} \sum_{\mathrm{j=1}}^{\mathrm{n_{ss,k}}} \left|\mathbf{w}_{u,i}^H \tilde{\mathbf{h}}_{\mathrm{k,j}}\right|^2 + N_0 \|w_{u,i}\|^2},$$

$$SINR_{u,i} = \frac{\left|\mathbf{w}_{u,i}^H \tilde{\mathbf{h}}_{\mathrm{u,i}}\right|^2}{\sigma_{\mathrm{u,i}}^2 + \varphi_{\mathrm{u,i}}^2 + \phi_{\mathrm{u,i}}^2} = \frac{\left|\rho_{j,i}\right|^2}{\Theta_{u,i}^2}, \quad (19)$$

where $\sigma_{\mathrm{u,i}}^2$ and $\varphi_{\mathrm{u,i}}^2$ denote the intra-stream interference and multi-user interference observed for the *j*th user at the *i*th SS. The Euclidian norm is denoted by $\|\cdot\|$.

Assuming that the interference and noise are Gaussian with zero mean and variance $\Theta_{j,i}^2$, then the maximum likelihood (ML) criterion for the *i*th SS transmitted to the *u*th STA is given by

$$\tilde{x}_{u,i} = \underbrace{min}_{\mathrm{x_{u,i}} \in \mathbb{C}} \left\| \frac{\tilde{y}_{u,i} - \rho_{u,i}\mathrm{s_{u,i}}}{\Theta_{\mathrm{u,i}}} \right\|^2 = \underbrace{min}_{\mathrm{x_i} \in \mathbb{C}} \frac{1}{\Theta_{u,i}^2} \left\| \tilde{y}_{u,i} - \rho_{u,i}\mathrm{s_{u,i}} \right\|^2. \quad (20)$$

Therefore, the Viterbi metric for soft-decision is given by

$$\mathrm{c_{u,i}} = \underbrace{min}_{\mathrm{x_i} \in \mathbb{C}} \frac{1}{\Theta_{u,i}^2} \left\| \tilde{y}_{u,i} - \rho_{u,i}\mathrm{s_{u,i}} \right\|^2 \quad for\ u = 1, \cdots, K;\ i = 1, \cdots n_{ss,u}, \quad (21)$$

where the Euclidian norm $\underbrace{min}_{\mathrm{x_i} \in \mathbb{C}} \left\| \tilde{y}_{u,i} - \rho_{u,i}\mathrm{s_{u,i}} \right\|$ is a r.v at the output of the soft demapper.

Neglecting the variation of the interference among the subcarriers, a simplified Viterbi metric can be stated as

$$\mathrm{c_{i,j}} = \underbrace{min}_{\mathrm{x_i} \in \mathbb{C}} \left\| \tilde{y}_{u,i} - \rho_{u,i}\mathrm{s_{u,i}} \right\|^2 for\ u = 1, \cdots, K;\ i = 1, \cdots n_{ss,u}. \quad (22)$$

Fig. 2 shows the packet error rate (PER) as a function of SNR in dB for *TGac D (4x2x4–SS1)* with IC-MMSE MIMO detector and TGac *D (4x1x4– SS1)* with MMSE MIMO detector. These results show that for the constant envelope modulation QPSK (MCS2) the use of Viterbi metrics that take into account the intra-stream interference, the MU-interference and the noise (Eq. 21) have the same performance with relation to (w.r.t.) the Viterbi metric that neglected these factors (Eq. 22). However, there are significant power losses when the simplified Viterbi metrics for the non-constant envelope modulation 16-QAM (MCS3) are used. Notice the significant performance degradation when hard-decision Viterbi decoding is implemented for both MCS with IC-MMSE MIMO detector. Finally, observe that the lack of information (i.e., complete CSI with information of all multiple users) originates an irreducible error floor when the MMSE MIMO detector without IC is implemented in systems with available spatial degrees of freedom to cancel the interference (i.e., when the number of receive antennas $n_{r,u}$ is greater than the number of SS $n_{ss,u}$).

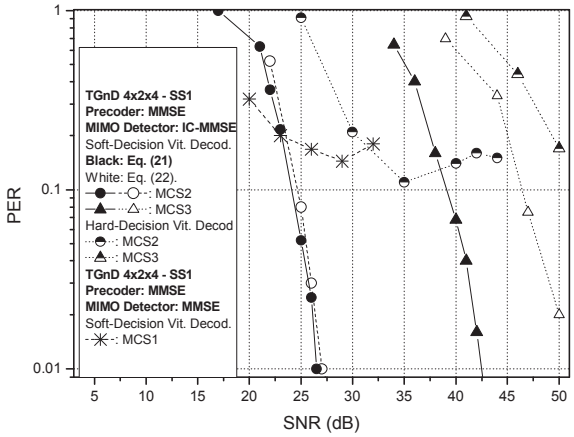

Figure 2. Effects of soft-decision Viterbi metrics on the PER as a function of SNR in dB over *TGac D 4x2x4–SS1* MIMO channel with RI-MMSE precoding and IC-MMSE MIMO detector.

B. IC-MMSE vs. MMSE MIMO Detectors

Fig. 3 shows that the IC-MMSE MIMO detector (*TGac D 4x2x4-1SS*) yields power gains of *1 dB* w.r.t. the plain MMSE MIMO detector (*TGac D 4x1x4-1SS*) for MCS0 and MCS1. However, when the code rate is decreased from 1/2 (MCS1) to 2/3 (MCS2) the IC-MMSE MIMO detector has a huge power gain of 10 dB w.r.t. MMSE MIMO detector. Notice that the rate of PER vs. SNR shows that diversity order decreases when the MMSE MIMO detector is implemented with MCS2 and MCS3. Both MIMO detectors present practically the same performance for a typical PER of 1% when a non-constant envelope modulation (MCS3) is assumed. Unfortunately, the performance of IC-MMESE MIMO detector with MCS3 degrades substantially w.r.t MMSE MIMO detector for a PER of 10%. Hence, we can infer that the use of non-constant envelope modulation with IC-MMSE MIMO detectors requires a robust interference cancellation scheme, whilst constant envelope modulation schemes present a significant less sensibility to error propagation due to imperfect cancellation of MU-MIMO interference.

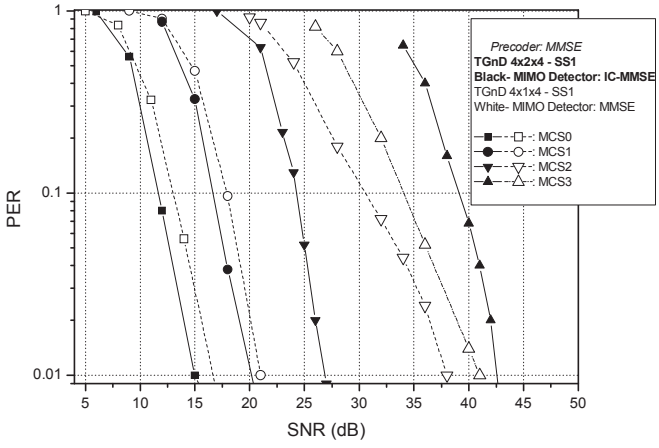

Figure 3. PER as a function of SNR in dB assuming RI-MMSE precoding and either IC-MMSE or MMSE MIMO detectors.

C. Channel Sounding Feedback Delay

Figures 4a (MCS0) and 4b (MCS2) are useful to compare the effects of outdated CSI information at transmitter side when the following MIMO detectors are implemented: *(i)* MMSE over a channel *TGac D (4x1x4-1SS)*; *(ii)* IC-MMSE over a channel *TGac D (4x2x4-1SS)*.

Fig. 4a shows that both IC-MMSE and MMSE MIMO detectors when it is implemented with one-dimensional constant envelope signaling scheme (BPSK) present robustness to feedback delays as high as *10 ms*. However, the power loss is increased significantly (*~3 dB*) and dramatically (*>7 dB*) for IC-MMSE and MMSE MIMO detectors, respectively, when the feedback delay is increased to *20 ms*. Finally, notice that the performance of IC-MMSE MIMO detector with delay of *10 ms* is equivalent to the performance of the plain MMSE MIMO detector with unrealistic instantaneous feedback.

In Fig. 4b, we investigate the effects of delay when the bi-dimensional constant envelope signaling scheme (MCS2) is transmitted over TGac D channels. Notice that now it is necessary to reduce the delay to *5 ms* in order that the power losses remain around *0.5 dB* and *1 dB* for IC-MMSE and MMSE MIMO detectors, respectively. When the feedback delay is increased to *10 ms,* a power loss of *3 dB* for IC-MMSE MIMO detector is observed. Note that this detector presents a highly superior performance w.r.t. the plain MMSE MIMO detector implemented assuming the hypothetical case of instantaneous feedback. Finally, we observe an error floor on the PER when the MMSE MIMO detector is implemented with a feedback delay of *10 ms*.

Fig. 5 compares the performance between the following configurations: *(i) TGac D (4x2x2-SS2)* with MMSE MIMO detector; *(ii) TGac D (4x2x4-SS1)* with IC-MMSE MIMO detector. If the MAC overheads (e.g., contention, sounding, ACK control frames) are not taken into account, then both systems have the same throughput since the first configuration transmits two SS to each one of two STA, whereas the second one transmits one SS to each one of four STAs. These results show that using one degree of freedom to cancel the interference allows a power gain of *5 dB* w.r.t. a MIMO system with MMSE and ideal instantaneous feedback. Notice that the performance of MMSE MIMO detector degrades completely when the feedback delay is of *10 ms*. The performance of IC-MMSE MIMO detector presents a power loss of only *2 dB* for *5 ms* delay. When the feedback delay is set to *10 ms*, the IC-MMSE MIMO detector still presents a superior performance w.r.t. MMSE MIMO detector without any delay.

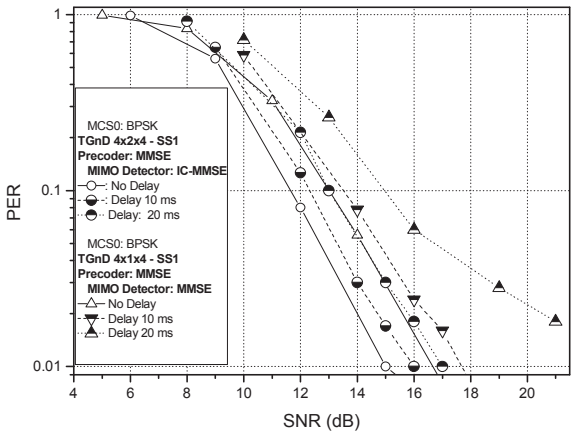

Figure 4a. Packet error rate vs. SNR for MCS0.

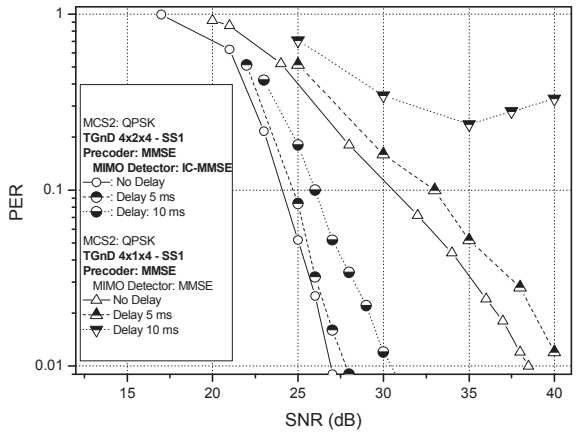

Figure 4b. Packet error rate vs. SNR for MCS2.

Figure 4. Effects of feedback delay on the performance of transceiver systems with RI-MMSE precoding and either IC-MMSE or MMSE MIMO detectors.

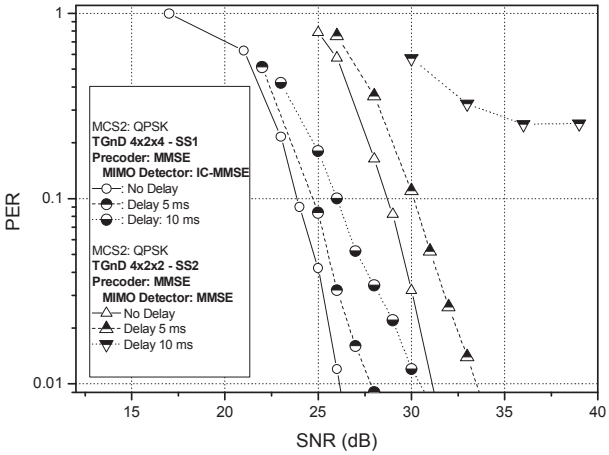

Figure 5. Effects of using spatial degrees of freedom to cancel the interference in 802.11ac MU-MIMO systems.

D. MU-MIMO vs. SU-MIMO with TxBF and Spatial Expansion

The spatial expansion (SE) technique, also known as (a.k.a) spatial spreading, uses fixed precoding matrices in order to avoid radio frequency power loss when the number of SSs is less than the number of transmit antennas. The SE matrices are not defined in 802.11ac standard amendment [1]. In this paper, we use the matrices proposed in [2, pp. 91], where each matrix has dimension n_t x n_{ss}. For instance, the precoding matrix at kth subcarrier for a SU-MIMO system with four transmit antennas used to transmit two SS is given by

$$\boldsymbol{P}_{SE,4x2}^{(k)} = \frac{1}{\sqrt{2}}\begin{bmatrix} 1 & 0 \\ 0 & 1 \\ \exp(-\mathrm{j}2\pi k\Delta f(-200\mathrm{ns})) & 0 \\ 0 & \exp(-\mathrm{j}2\pi\Delta f(-200\mathrm{ns})) \end{bmatrix}, \quad (23)$$

where Δf denotes the spacing between subcarriers.

The matrix $\boldsymbol{H} = \boldsymbol{U}\boldsymbol{\Lambda}\boldsymbol{V}^{\boldsymbol{H}}$ is the singular value decomposition (SVD) of the SU-MIMO channel, where $\boldsymbol{U} \in \mathbb{C}^{n_r \times n_r}$ and $\boldsymbol{V} \in \mathbb{C}^{n_t \times n_t}$ are unitary matrices. $\boldsymbol{\Lambda} \in \mathbb{C}^{n_r \times n_t}$ is a matrix with dimension n_r by n_t, whose diagonal elements are the non-negative real singular values of the MIMO channel matrix **H** and whose non-diagonal elements are zero [8]. In this paper, the SU-MIMO TxBF transceiver architecture implements the precoder using the matrix **V** at TX side and the MMSE equalizer is implemented at the RX side. Hence, the signal at the MIMO detector output is given by

$$\tilde{\mathbf{y}} = \boldsymbol{W}_{MMSE}^{H} \cdot (\mathbf{HVs} + \mathbf{z}) = \boldsymbol{W}_{MMSE}^{H} \cdot (\mathbf{UHV}^{\mathbf{H}}\mathbf{Vs} + \mathbf{z}),$$
$$\tilde{\mathbf{y}} = \boldsymbol{W}_{MMSE}^{H} \cdot (\mathbf{UHs} + \mathbf{z}) = \boldsymbol{W}_{MMSE}^{H}\hat{\mathbf{H}}\mathbf{s} + \boldsymbol{W}_{MMSE}^{H}\mathbf{z}. \quad (24)$$

Tab. III compares our 802.11ac simulation results w.r.t the ones shown in [2, pp. 394], where TxBF over TGac D 4x2 SU-MIMO channel is assumed. There is a mismatch of approximately *1.5* to *2.5 dB* between both simulation results. Notice that 802.11n/ac simulators are extremely complex since a multitude of signal processing operations are involved (from channel modeling to phase tracking) and we have not obtained the full details of the simulator implemented in [2], since only generic information is available (e.g., *"Synchronization, channel estimation and phase tracking are included in the simulation*" [2, pp. 393]). Finally, we emphasize there are not any results of PER as a function of SNR for MU-MIMO in the 802.11n/ac design book [2].

Table III. Comparison between the SNR necessary to obtain a PER of 1%.

	Simulation	Ref. [2]		Simulation	Ref. [2]
MCS0	9.0 dB	7.5 dB	MCS5	25.0 dB	23.0 dB
MCS2	15.5 dB	14.0 dB	MCS6	28.0 dB	26.5 dB
MCS4	22.5 dB	20.0 dB	MCS7	31.0 dB	28.5 dB

Fig. 6 investigates comparatively the performance of the following 802.11ac transceiver architectures: *(i)* MU-MIMO with IC-MMSE MIMO detector over *TGac D (4x2x4-SS1)* channel; *(ii)* SU-MIMO with TxBF over *TGac D (4x2x1-SS2)* channel model; *(iii)* SU-MIMO with SE over *TGac D (4x2x1-SS2)* channel model.

The following analyzes of link throughput do not take into account the MAC overheads. First, Fig. 6 shows that the SU-MIMO TxBF system using MCS5 has a throughput of *468 Mbps* (see Tab. II) with a SNR of *25 dB* for a PER of 1%, whereas the MU-MIMO system using MCS2 has a throughput of *351.2 Mbps* (*4 x 87.8 Mbps*). Second, we verify that if the SNR is increased to *28 dB*, then the SU-MIMO TxBF system presents a link throughput of *526.5 Mbps* using MCS6 (cf. Tab. II). Third, we see that a feedback delay of *20 ms* originates power losses of *0.5 dB* and *1.5 dB* for MCS5 and MCS6, respectively, for the SU-MIMO TxBF system. For the MU-MIMO system, a delay of *5 ms* generates a power loss of *0.5* dB for MCS2. Notice that the MU-MIMO with MCS3 needs an unfeasible SNR of *42.5 dB* to get o PER of *1%*. Finally, we observe that the SE configuration has a dramatic power loss *of 12 dB* w.r.t. SU-MIMO TxBF system when the MCS5 is used.

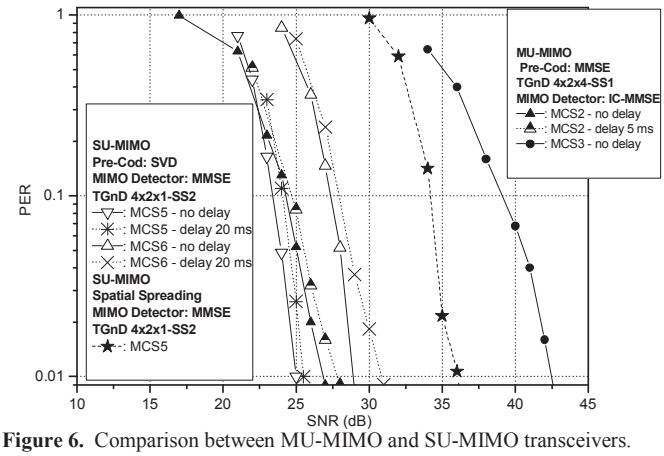

Figure 6. Comparison between MU-MIMO and SU-MIMO transceivers.

IV. CONCLUSIONS

In this research and design (R&D) industrial oriented paper, we have developed PHY signal processing techniques used in implementation of MU-MIMO 802.11ac transceivers with regularized channel inversion MMSE precoder and IC-MMSE MIMO detector.

First, we described the motivations that drive the implementation of interference cancellation techniques in the framework of MU-MIMO in 802.11ac systems. Second, we developed in great detail the received signal model for the downlink MU-MIMO; the sounding and channel estimation procedures specified in the 802.11ac amendment; the Doppler power spectrum defined in the TGac spatial-correlated and frequency selective MIMO channel models; the MU-MIMO precoding based on regularized channel inversion MMSE; and the interference cancellation MMSE MIMO detector. Third, after defining our IEEE 802.11ac simulator framework, we presented a consistent set of simulation results to investigate the performance of the aforementioned transceiver techniques in the context of IEEE 802.11ac systems.

We have concluded that the implementation of IC-MMSE MU MIMO detectors is a fundamental challenging issue in order to mitigate the performance degradation due to both imperfect CSI and feedback delays of the 802.11ac sounding procedure. We also have verified that the application of adaptive transmit beamforming in SU-MIMO 802.11ac presents significantly less sensibility regarding staled channel state information in relation to MU-MIMO techniques. Finally, we have shown that fixed TxBF based on spatial spreading presents a severe power loss in relation to adaptive transmit beamforming.

REFERENCES

[1] Wireless LAN Medium Access Control and Physical Layer Specifications, Amendment 5: Enhancement for Very High Throughput for Operations in Bands below 6 GHz. IEEE P802.11ac, Dec., 2013.

[2] E. Perahia and R. Stacey, *Next Generation Wireless LANS*: *802.11n and 802.11ac.2th ed*. Cambridge: Cambridge University Press, 2013.

[3] VK Jones and H. Sampath. "Emerging technologies for WLAN," in *IEEE Communication Magazine,* vol. 53, no. 3, pp. 141-149, March, 2015.

[4] S. Veramani and A. V. Zelst, *Interference cancellation for downlink MU-MIMO*. IEEE 802.11-09/1234r1, 2010.

[5] J. Park et. al. "A high performance MIMO detection algorithm for DL MU-MIMO with practical errors in IEEE 802.11ac systems," in *2013 IEEE 24th Symp. on Personal, Indoor and Mobile Radio Communications,* 2013.

[6] W. Lin et. al. "Performance of linear precoding and user selection in IEEE 802.11ac downlink MU-MIMO system," in *2014 IEEE Wireless Communications and Networking Conference (WCNC),* Istanbul, 2014.

[7] H. Yu, O. Bejarano and L. Zhong. "Combating inter-cell interference in 802.11ac-based MIMO networks, " in *Proc. of the 20th Annual International Conference on Mobile Computing and Networking (MOBICOM'14),* 2014.

[8] Y. S. Cho, J. Kim, W. Y. Yang and C. G. Kang, *MIMO-OFDM Wireless Communications with MATLAB*. Singapore: John Wiley & Sons, 2010.

[9] O. Bejarano, E. Magistretti, O. Gurewitz and E. Knightly, "MUTE: Sounding inhibition for MU-MIMO WLANs," in *2014 11th Annual International Conference on Sensing, Communication and Networking,* 2014.

[10] C. B Peel, B. M. Howhwald and A. L. Swindlehurst. "A vector - pertubation technique for near-capacity multi antenna multiuser communication - Part I: channel inversion and regularization," in *IEEE Transactions on Communications*, vol. 53, no. 1, pp. 195-202, Feb. 2005.

[11] G. Breit, H. Sampath, S. Vermani, et. al., *TGac Channel Model Addendum Support Material.* IEEE 802.11-09/06/0569r0, May 2009.

[12] R. P. F. Hoefel. "Multi-User OFDM MIMO in IEEE 802.11ac WLAN: a simulation framework to analysis and synthesis", in *IEEE Latin America Transactions,* vol.13, no. 2, pp.540-545, Feb. 2015.

[13] F. Tosato and P. Bisagli, "Simplified soft-output demapper for binary interleaved COFDM with applications to HIPERLAN/2," *IEEE International Conference on Communications 2002*, 2002.